Using Green's function molecular dynamics to rationalize the success of asperity models when describing the contact between self-affine surfaces

Carlos Campañá*
CANMET—Materials Technology Laboratory, Natural Resources Canada, Ottawa, Ontario, Canada K1A 0G1
(Received 30 April 2008; published 18 August 2008)

We use Green's function molecular dynamics to evaluate the effectiveness of asperity models when describing the contact mechanics of elastic solids with self-affine surfaces. Surfaces are created with the help of a Fourier filtering algorithm, and the interactions between the solids are modeled via hard-wall potentials. We illustrate how the real area of contact A_{real} is formed by a set of contact clusters. Two different regimes are identified when the normal force per cluster L_c is plotted as a function of its area A_c. Small clusters satisfy a Hertzian-type law $L_c \sim A_c^{3/2}$, while large clusters display a linear $L_c \sim A_c$ behavior. It is shown how the area A_c^*, where the crossover between the two regimes takes place, depends only on the roughness at the smallest length scale if the longitudinal dimension of the surface remains unaltered. Moreover, our results display a distribution of cluster sizes $P(A_c)$ remaining nearly constant for areas smaller than A_c^*, while showing power law decay above such a critical value. Furthermore, we found the heights of the contacting atoms to be normally distributed with width inversely proportional to the surface roughness.

DOI: 10.1103/PhysRevE.78.026110 PACS number(s): 81.40.Pq, 45.10.−b, 02.70.−c

I. INTRODUCTION

Asperity models have ruled the field of analytical theories developed to describe the contact mechanics of rough surfaces since the publication of the ground-breaking paper by Greenwood and Williamson in the mid-1960s [1]. The need for understanding and predicting the nature of the contact between rough surfaces stems from its many potential applications in industry [2,3]. Over the last 40 years, due to their success in describing rough contacts, asperity models have become tools of common engineering practice to estimate the values of many physical variables at the interface between contacting solids. The real area of contact, friction, adhesion, electrical conductance, and wear are just a few examples of the several variables scientists and engineers have studied using such models [4–7].

Analytical solution of the equations of linear elasticity for the contact problem of rough surfaces is currently an impossible task [8]. In order to predict the contact mechanics of rough surfaces all asperity models have to rely on certain approximations and assumptions. The one exception is the case where the surfaces consist of leveled regular arrays of parabolic bumps which can be solved exactly using the Hertz contact theory [9]. Otherwise, in most cases, three main postulates have to be introduced, regardless of the specific characteristics of the given model. As a first postulate, it is assumed that all surfaces are formed by a set of asperities (bumps), which individually satisfy the Hertzian contact mechanics. That is, when contact occurs, the load L_c and the area A_c per asperity are related such that $L_c \sim A_c^{3/2}$.

The asperity definition itself has proven very controversial [10,11]. Within the theory of Greenwood and Williamson (GW) [1], an asperity is considered to be a spherical bump with curvature radius R. Thus, the surface consists of an array of identical bumps arranged in a way that their heights are distributed according to a Gaussian law. A variation of the GW model, developed by Bush, Gibson, and Thomas [12], has proposed each asperity to be a parabolic bump and the surface a collection of those bumps with a height distribution that can be described by a random process. Further attempts within similar models to approach the shape of real surfaces [13–15] have introduced a distribution of asperity sizes. Yet individual asperities are considered by these latter models as being described using quadratic functions and such that individually they satisfy the Hertzian contact mechanics. While well aware of the limitations of the asperity definition in tackling the resolution dependence of real surfaces, all the authors of asperity models seem to agree with the validity of the Hertzian contact mechanics at the single-asperity level.

The second assumption commonly used by these theories is to consider nominally smooth geometries, which is a reasonable conjecture at enough large scales. More specifically, they suggest that the height distribution of real surfaces can be approximated by a Gaussian law. Certainly, many experimental works show a wide range of real surfaces displaying the aforementioned characteristic [3,16]. Questioning the validity of this second assumption has been the aim of some recent studies [17–19], but the effect of non-Gaussianity in the height profiles is generally found to be small. Moreover, because there exist many computational techniques known to us to generate surfaces with Gaussian distributed heights [20], this particular supposition makes the predictions of asperity models more amenable to comparison with those of numerical simulations [21].

The third postulate, which classifies more as a limitation than an advantage of asperity models, relates to neglecting the effects of long-range elastic interactions within the contact region. That is, if a certain asperity gets pressed down at a given time, the neighboring asperities will not experience any elastic perturbation at their locations. It is important to note that such behavior does not depend on the distance between asperities. Therefore, the elastic response of the neigh-

*ccampana@nrcan.gc.ca

boring bumps is uncorrelated with the action exerted on the bump at the origin. The limitations associated with this postulate have been extensively discussed within prior works of the current author [2,22] as well as by other groups [23,24].

Using computer simulations, several experts have studied the variations in the contact morphology as a result of considering long-range elastic interactions [23–27]. The main advantage of the simulations, as opposed to theoretical approaches, is that they can numerically solve exactly the elastic contact problem of rough surfaces. Robbins and colleagues [23,24,26] have found that correlations in the positions of contacting asperities affect the size and the distribution of the contact regions. They have also analyzed the effects of roughness at large and small wavelengths in the nature of the contact between randomly rough surfaces [23]. Batrouni *et al.* [25] and Borri-Brunetto *et al.* [27] have looked into the dependence of the real area of contact A_{real} as a function of the applied load. However, they focused more on the effects of increasing the resolution in the roughness of the surfaces rather than in the long-range elastic coupling at the interface.

In a previous contribution [2], the current author and collaborators showed how the lack of long-range correlations in asperity models limits tremendously their prediction capabilities when the shapes of the surfaces under study are no longer randomly rough. Nevertheless, the assumptions of asperity models appear to work reasonably well for surfaces with several decades in roughness whenever the applied load is low enough and their topographies can be described using a Gaussian height probability distribution.

In this paper we applied the Green's function molecular dynamics technique [28] to study the elastic contact problem of rough surfaces with self-affine topographies. We show how the area of contact is formed by a set of contact clusters and we study their size and height distributions. Two different scaling regimes are identified when the normal force per cluster L_c is plotted as a function of its area A_c. The way that variations in the roughness of the surfaces are reflected in the shape of the area probability distribution $P(A_c)$ of the clusters is also discussed. We have also calculated what percentage of the total contact area is occupied by each one of the two scaling regimes referred to above. Our results proved to be robust when the resolution of the numerical grid employed to model the elastic solid was increased.

The remainder of the manuscript is structured as follows. In Sec. II we review the technical aspects of our numerical approach. Whenever required, reference is made to the original contributions for a more exhaustive analysis of the methodology. In Sec. III we present the simulation results and use them to rationalize the success of asperity models for self-affine surfaces. Conclusions are drawn in Sec. IV.

II. NUMERICAL METHODS

As in previous work [24,28–30], we use a well-known contact mechanics mapping model to simplify the problem of bringing two elastic bodies with rough surfaces into contact. In the absence of friction, adhesion, and sliding, the problem of normal elastic contact between two self-affine surfaces can be mapped into the problem of the contact between a rigid composite topography and an elastic plane [8]. Two properties ensure the exactness of such a mapping model. First, the power spectra $\tilde{h}(\mathbf{q})$ of self-affine surfaces is additive. Second, the effective elastic modulus E' of the equivalent plane is uniquely determined from the elastic moduli $E_{1,2}$ of the two solids initially brought into contact.

The elastic solids considered in this study are modeled as a single plane (sheet) of atoms, where the renormalized forces between the atoms are computed with the help of a Green's function formalism [28,31]. The Green's function formalism allows for a coarse-grained representation of a full harmonic solid, in which the bulk elastic interactions have been integrated out. For a more complete analysis we suggest a review of the original paper in which the technique was introduced [28].

The masses of the atoms forming the elastic sheet are chosen to be identical, $m=1$. The lattice constant of the elastic manifold is set to $a=1$ and the renormalized interactions are defined such that both Lamé constants λ and μ are unity. This is equivalent to making the sheet's elastic modulus $E=5/2$, its bulk modulus $K=5/3$, and its Poisson ratio $\nu=1/4$.

Self-affine topographies were produced using a Fourier filtering technique for the heights $\tilde{h}(\mathbf{q})$ [20]. With its help, we generated surfaces with Gaussian distributed heights. Such a distribution has expectation value and second moment satisfying

$$\langle \tilde{h}(q) \rangle = 0, \tag{1}$$

$$\langle \tilde{h}^*(q)\tilde{h}(q) \rangle = h_s^2 (q_s/q)^{2H+2} \theta(q_s - q)\,\theta(q - q_l), \tag{2}$$

where h_s is the amplitude of the roughness at the short wavelength. $\theta(\cdot)$ is the Heaviside step function and q_s and q_l are the corresponding cutoffs characterizing the short- and long-wavelength roughness. In this study, the roughness vector $q_l = 2\pi/\lambda_l$ is defined such that $\lambda_l = \mathcal{L}$, $\mathcal{L}$ being the longitudinal dimension of the interface. Unless stated, in all simulations the ratio $\lambda_l/a = 4096$. Because the dimensions of the interface remained fixed, only the vector q_s was allowed to change. The variable H is known as the roughness (or Hurst) exponent. In this work, the values of H, h_s, and q_s are changed within the definition of the second moment $\langle \tilde{h}^*(q)\tilde{h}(q) \rangle$ such that the root-mean-square gradient of the surfaces remained constant, $\sqrt{\langle \{\nabla h(\mathbf{r})\}^2 \rangle} = 0.031$. This permitted us to work within the small-slope approximation when comparing our numerical results to the predictions of asperity models, as required by the theory of linear elasticity [32].

To mimic the interactions between the elastic plane and the rigid self-affine substrate, hard-wall potentials are employed. We use a hard-wall approach that acts as a boundary condition, preventing the elastic plane from penetrating the rigid rough surface at all times. As mentioned in previous contributions [28,33], this boundary condition can be enforced by setting the normal coordinate of any atom that penetrates the surface, to the value of the surface height $h(\mathbf{r})$ corresponding to the same in-plane vector $\mathbf{r}$. In addition, the

direction of the normal component of the velocity of the atom should be reversed. It is worth mentioning that this artificial implementation of hard-core potentials does not affect the results of the simulations, when compared to other standard approaches, as long as one is not interested in dynamics.

Identifying the atoms in contact at the interface, as well as labeling the different contact clusters, is done by means of the Hoshen-Kopelman (HK) algorithm [34]. The HK algorithm defines each contact cluster by considering all those atoms that are "in contact" and can be connected through a continuous path of nearest neighbors in a square lattice. Other labeling techniques could be considered; however, the current implementation facilitates the comparison of our results to those obtained by Pei *et al.* [26] and Hyun *et al.* [23,24], who used an identical labeling technique.

III. RESULTS

A. The definition of contact: Cluster morphology

Definition of which regions are in contact between two solids involves a nontrivial analysis within experiments as well as in numerical simulations. Past experimental works [35] have used optical methods to visualize and determine the contact area. The criterion employed by Dieterich *et al.* [35] to differentiate between the conditions of "contact" and "no contact" was to identify as in contact any region where the surfaces were closer than some fraction of the wavelength used by their optical system. However, as suggested by Hyun *et al.* [24], due to the fractal nature of the contact in the Dieterich *et al.* experiments, such a criterion might have resulted in an overestimation of the real area of contact.

If the interactions between the surfaces are modeled using finite-range potentials, the definition of contact can be challenging also within computer simulations. Yang *et al.* [30] have noticed that neither the criteria of a *critical distance* nor a *critical pressure* are good enough to define contact whenever finite-range interactions are considered. For example, for a parabolic asperity, the critical pressure or distance establishing where contact takes place depends on its radius of curvature. Above, it is assumed that such *critical magnitudes* are computed by fitting the Hertzian pressure profile to the numerical data. Similar arguments apply to surfaces with roughness on many length scales, in which one encounters a large number of asperities conforming the topographies.

Alternatively, when the nature of the interactions between the solids are modeled via hard-core potentials, the contact area can be defined as those regions where the surfaces overlap. A procedure of this kind, based on geometrical considerations, was chosen by Robbins and colleagues [23,24] in their finite-element approach. However, we have employed a different criterion to define contact within the context of this work. In our model, an atom is expected to be in contact if the pressure acting on such a particle exceeds some predetermined value. Thus, the results we report in this paper correspond to those obtained once convergence is achieved after the values of this pressure threshold are decreased continuously.

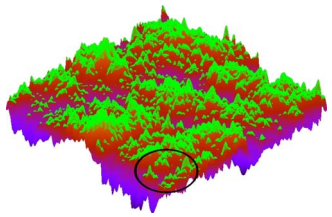

FIG. 1. (Color online) Visualization of a self-affine surface and contact clusters (light colored regions). The surface shown can be characterized by a roughness exponent $H=0.3$, a relative roughness ratio $q_s/q_l=64$, a discretization ratio $q_a/q_s=64$, and a rms gradient of 0.031.

If two elastic solids are brought into contact via Green's function molecular dynamics (GFMD), once equilibrium is achieved, the real area of contact appears to be formed by a set of contact clusters of variable size as shown in Fig. 1. Small clusters have geometries that resemble those of parabolic tips while larger clusters display more complex topographies. It is the competition between the roughness ratio q_s/q_l and the discretization ratio q_a/q_s that determines the nature of the contact clusters. Above it is assumed that $q_a=2\pi/a$. The roughness ratio describes how much larger is the longest wavelength where roughness exists, as compared to the short roughness wavelength within the fractal surface. Conversely, the discretization ratio is a measure of how many atoms are found per short roughness wavelength, or, in other words, how many atoms on the elastic plane occupy the area of a single parabolic tip on the self-affine surface. We name the product of the roughness and discretization ratio the resolution ratio q_a/q_l.

The effects of changing the discretization (resolution) in rough contacts, have been discussed extensively in the recent works of several authors [2,23,24,29,36]. To allow a proper comparison between the results of GFMD simulations and the predictions of asperity models for surfaces with multiscale roughness, two major requirements have to be satisfied. First, the discretization of the elastic plane at the single-asperity level has to be such that the pressure probability distribution $P(p)$ approaches zero as the pressure decreases, i.e., $P(p)\to 0$, $p\to 0$. This condition ensures that the resolution of the elastic sheet is such that there are sufficient atoms per individual Hertzian tip to reproduce correctly its analytical solution [8]. If the $P(p)$ remains unchanged after further increase in the discretization of the elastic sheet, we call it a *converged* pressure distribution. Second, the number of asperities that form the surface has to be large enough in order for the results to be self-averaging. Statistically speaking, the theoretical assumption of a nominally flat surface can only be achieved in our numerical simulations when $q_s/q_l \geqslant 64$.

B. Distribution of normal forces

The distribution of normal forces over the full set of contact clusters constitutes a subject of interest when the contact mechanics of self-affine surfaces is studied. We mentioned in the Introduction of this paper that the first assumption of most asperity models is to approximate the area of contact

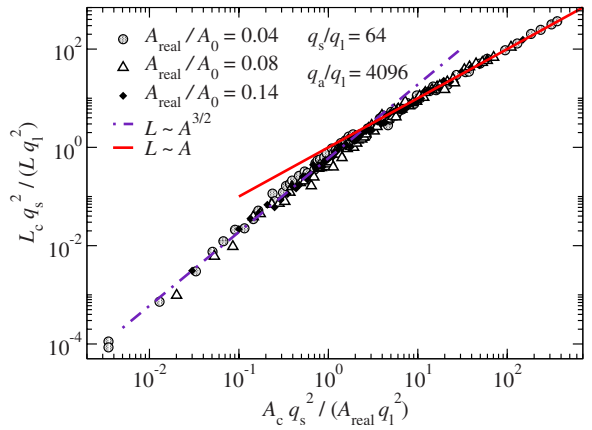

FIG. 2. (Color online) Load per contact cluster (L_c) as a function of its area (A_c) for different values of the real area of contact A_{real}. The plot corresponds to a self-affine surface characterized by a roughness exponent $H=0.3$, a relative roughness ratio $q_s/q_l=64$, a discretization ratio $q_a/q_s=64$, a resolution ratio $q_a/q_l=4096$, and a rms gradient of 0.031. The continuous line shows the linear region $L_c \sim A_c$ while the dashed line displays the Hertzian $L_c \sim A_c^{3/2}$ regime. Both axes have been normalized such that different plots collapsed onto one universal curve.

with a group of disconnected asperities which individually satisfy the Hertzian contact mechanics. To test this assumption, in Fig. 2 we have plotted the normal load per contact cluster L_c as a function of its area A_c. The discretization ratio for this case was $q_a/q_s=64$. This value proved to be sufficient to obtain numerically converged pressure histograms. In the plot, both axes were normalized in such a way that the results of simulations corresponding to different relative areas of contact, A_{real}/A_0, are superimposed. Here A_0 stands for the total area of the surface. The normalization factor we used, $(q_s/q_l)^2$, is motivated by recent work of Hyun and Robbins [23]. In their contribution, the authors reported the existence of two scaling regimes in the area probability distribution $P(A_c)$ of the contact clusters. The transition point between the two regimes seemed to be only a function of the short-scale roughness; hence our choice for the normalization factor. Each data point included within Fig. 2 represents an average over ten clusters of the original size distribution. Lastly, to guarantee that we worked in the limit of small loads, the values of the relative contact area A_{real}/A_0 were varied up to a maximum value of $\approx 14\%$.

Two different regions are identified within Fig. 2 in the distribution of normal forces. For clusters of small sizes, a Hertzian-type regime in which $L_c \sim A_c^{3/2}$ becomes clearly visible. In opposition, clusters of large area appeared to follow a linear law $L_c \sim A_c$. As expected, we observed how the average distribution of small clusters can be modeled using the Hertzian contact mechanics. This is due to the fact that at small scales single asperities are fully resolved within our simulations. However, the existence of a Hertzian and a linear regime within the interface emerges as a new feature that has not been reported until recently by the current author and collaborators [22]. The linear behavior at larger scales is the result of roughness with many different wavelengths forming the contact region, which makes the load scaling with area similar to that of the macroscopic contact area.

Clearly, the presence of the linear clusters does not compromise the capabilities of asperity models when predicting the linear relation between applied load and total contact area at small loads. If the contribution of the asperities in the Hertzian region accounts for the linear relationship between the real area of contact and the applied load, certainly inclusion of the contribution of the asperities in the linear region will not change the outcome. However, the nature of the contact results in a more complex topology in which not one, but two, different scaling regimes coexist. We chose to name the area A_c^* at which the crossover takes place the *critical area*.

Understanding the dependency of the critical area with respect to the variables characterizing the contact comprises the purpose of the following paragraphs. From analytical theories [1,12,37], it is well known that the real contact area A_{real} and the total applied load L are related through the equation

$$A_{\text{real}} = \frac{\kappa}{\sqrt{\langle \{\nabla h(\mathbf{r})\}^2 \rangle}} \frac{L}{E'}, \tag{3}$$

where κ is a dimensionless proportionality coefficient, $E' = E/(1-\nu^2)$ is the effective elastic modulus, and E and ν are the Young's modulus and the Poisson ratio, respectively. The remaining term in the denominator corresponds to the surface's root-mean-square gradient as already mentioned in Sec. II. Note that, if we fix the elastic properties of the solid as well as the surface topography, A_{real} and L will be related through a unique proportionality constant.

Combining the results shown in Fig. 2 with Eq. (3) allows us to obtain approximate scaling laws for A_c^*. The x axis on the graph shows the crossover occurring approximately at the same value of A_c^* for all the different cases. This universal crossover condition reads

$$\frac{A_c^*}{A_{\text{real}}} \left(\frac{q_s}{q_l} \right)^2 \sim c, \tag{4}$$

with c being a constant such that $c \approx 2$. With the help of Eqs. (3) and (4) the scaling law for the critical area adopts the form

$$A_c^* \sim \frac{\kappa c}{\sqrt{\langle \{\nabla h(\mathbf{r})\}^2 \rangle}} \frac{L}{E'} \left(\frac{q_l}{q_s} \right)^2. \tag{5}$$

Equation (5) explicitly includes the possibility of a similar superposition for different graphs, when the ratio $(q_s/q_l)^2$ and not A_{real} becomes the magnitude experiencing changes. Moreover, an almost identical value for the constant c should be expected. Indeed, that is exactly what we observe when the data from these calculations is plotted following the same approach used to produce Fig. 2. The results of the new simulations are included within Fig. 3. In this version of the plot, we have kept the relative area of contact constant and only varied the fraction $(q_s/q_l)^2$ such that the rms gradient of the surface remains unchanged. The roughness exponent, the discretization ratio q_a/q_s, the elastic properties of the sheet,

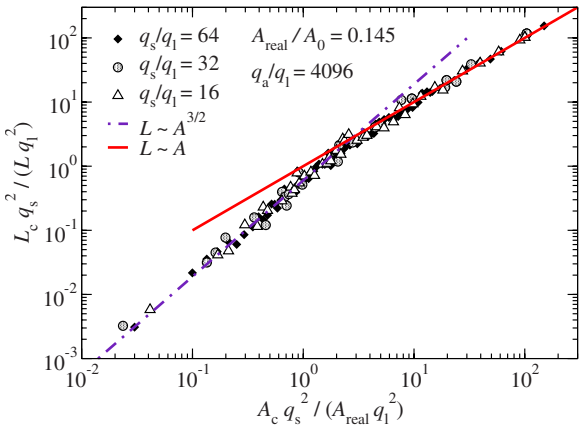

FIG. 3. (Color online) Load per contact cluster (L_c) as a function of its area (A_c) for different values of the roughness ratio q_s/q_l. The plot corresponds to a self-affine surface characterized by a roughness exponent $H=0.3$, a resolution ratio $q_a/q_l=4096$, a relative contact area $A_{real}/A_0=0.145$, and a rms gradient of 0.031. The linear $L_c \sim A_c$ (Hertzian $L_c \sim A_c^{3/2}$) regime is shown using a continuous (dashed) line. Both axes have been normalized such that different plots collapsed onto one universal curve.

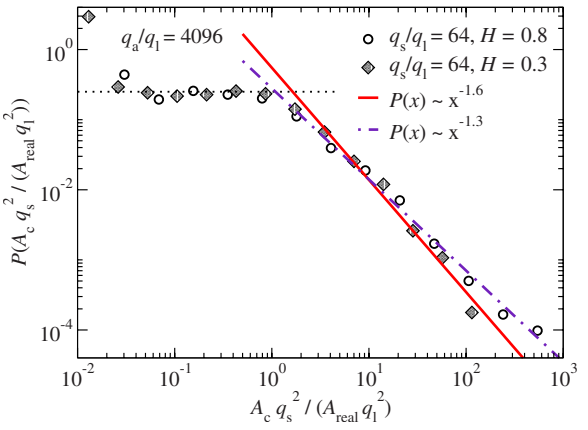

FIG. 4. (Color online) Area probability distribution of the contact clusters, $P(A_c)$, for a given roughness ratio ($q_s/q_l=64$). A nearly constant $P(A_c)$ is seen for small clusters while a power law scaling is identified for large cluster sizes. When the value of the roughness exponent H is increased, the nearly constant probability distribution remains unaltered, while the power law at large sizes shifts its exponent to lower values in absolute units.

and the random seed employed to generate the surface also remained unaltered. Simulations corresponding to other values of the roughness exponent displayed identical features.

C. Area and height probability distributions

As mentioned within Sec. II, variations in the ratio q_s/q_l in this work were achieved by changing only the short-scale roughness q_s while keeping fixed $q_l=2\pi/\lambda_l$, where $\lambda_l=4096a$. With this in mind and looking back to Figs. 2 and 3, one can conclude that, if the longitudinal dimension $\mathcal{L}$ of the interface is constant, the critical area of the contact clusters depends only on the short-scale roughness. In their paper, Hyun *et al.* [23] reached a similar conclusion by looking at the probability of finding a contact cluster of a given area $P(A_c)$. Although the authors did not analyze the distribution of normal forces on the contact regions, they found two different scaling regimes for $P(A_c)$. The area where the transition from one regime to another took place proved to be a function of only the small scale where roughness existed.

Our results concerning the computation of the area probability function for the contact clusters are stated in Fig. 4. As in the paper by Hyun *et al.* [23], we found two regions in which $P(A_c)$ obeyed different trends. In the first region, associated with the Hertzian regime, $P(A_c)$ stayed almost constant. In contrast, in the linear regime the probability function decayed following a power law. The results presented correspond to the same surface employed to generate the plots in Figs. 2 and 3. Additionally, we have included data points corresponding to simulations performed with a value of the roughness exponent $H=0.8$. This is due to the fact that most of the real surfaces can be described by a Hurst exponent close to 0.8.

Figure 4 shows how, after the value of H was increased, the $P(A_c)$ for small clusters hardly changed. Conversely, for clusters of large area the exponent of the power law becomes smaller in absolute units. Having a $P(A_c)$ at small cluster sizes independent of the roughness exponent is related to the fact that each single asperity is fully resolved within the simulations. The geometry of clusters with sizes of the order of the short wavelength λ_s^2 cannot be a function of the Hurst exponent characterizing the self-affine nature of the surface topographies. In self-affine fractals, the rms gradient of the surface scales as $\ell^{-(1-H)}$ [20], with ℓ being the distance that characterizes lateral variations in the heights. For surfaces with $H<5$ this results in anticorrelation between surface slopes in neighboring regions. Alternatively, when $H>5$ positive correlation between local slopes arises [24], leading to a $P(A_c)$ that depends on H at large areas. One should expect from such differences that smaller Hurst exponents would limit the formation of large clusters, as verified above in our Fig. 4. Hyun and Robbins [23] arrived at a similar conclusion when studying the effects of changing the large-scale roughness q_l in self-affine systems. However, we consider it important to highlight that the resolution of our numerical grid is significantly higher than any of those used in the past for contact mechanics problems. Previous meshes allowed for a total number of 512×512 grid points at the interface [23–25], while with our method we take the prior value up to 4096×4096 system sizes. The possibility of modeling such large sizes allowed us to resolve features in these systems unable to be captured by any of the prior numerical works.

We have also looked at the modifications that $P(A_c)$ undergoes with changes in the roughness ratio q_s/q_l. The outcome of this second group of simulations is presented in Fig. 5. In the language of asperity models, increasing the roughness ratio results in an increment in the number of asperities that form the surface topography. Consequently, to maintain the same rms gradient of the surface, one has to reduce the amplitude of the fluctuations in the height profile. A larger number of asperities implies that higher resolution should be used in order to obtained *converged* pressure histograms. As

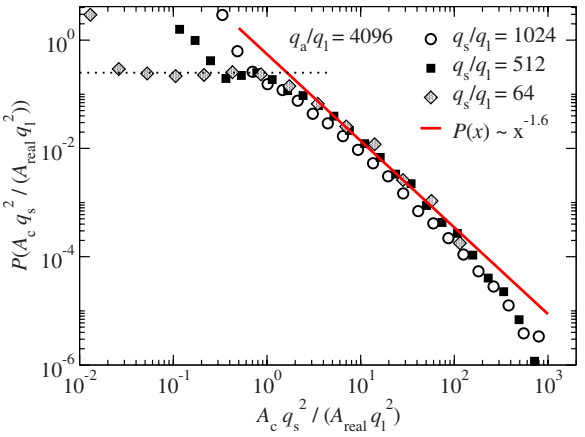

FIG. 5. (Color online) Area probability distribution of the contact clusters for a given roughness exponent (H=0.3). When the roughness fraction is reduced (the value q_s/q_l is decreased), the nearly constant probability distribution becomes clearly visible for clusters with sizes of the order of (or smaller than) of the small roughness wavelength found within the surface.

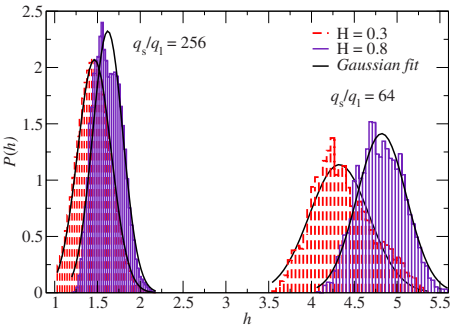

FIG. 6. (Color online) Height probability distribution of the contact clusters for two different values of the roughness ratio q_s/q_l =64 and 256. The Hurst exponents of the topographies are H=0.3 (red broken bars) and H=0.8 (indigo continuous bars). The rms gradient of the surfaces are identical in all cases (0.031). At the highest discretization ratio q_a/q_s=64 (corresponding to the lowest value of q_s/q_l because the resolution ratio is constant, q_a/q_l =4096 for all simulations), the distribution has the greatest width. The continuous black lines correspond to Gaussian fits to the numerically simulated data.

we are limited to system sizes of 4096×4096, only the histograms corresponding to a ratio q_s/q_l=64 showed full convergence. That is the reason why within Fig. 5 the $P(A_c)$'s at small cluster sizes appear to be nearly constant only for the q_s/q_l=64 case.

Variations in the roughness ratio did not affect significantly the exponent of the $P(A_c)$ power law in the region of large clusters. The trend was also observed by Hyun *et al.* [23,24] though the exponent of the power law they reported deviates from the value we obtain for a similar case. We believe the reason for this discrepancy lies in a fundamental difference between our models. The model of Hyun *et al.* considered the flat substrate to be rigid while the finite-element mesh was assigned to the rough elastic solid. In contrast, we located the mesh on the elastic plane while the rough surface was assumed to be rigid. For discrete models, there is no requirement within the elasticity theory that suggests the two approaches are equivalent. As a matter of fact, if one imagines the contact mechanics of a parabolic tip, the morphology of the contact will turn out to be quite different in the two cases. Hyun's *et al.* framework would show a tip that flattens at the top when contact takes place with the rigid plane. Our model would visualize the elastic plane deforming while getting closer to the base of the tip as contact occurs.

How are the heights of the contacting regions distributed at the interface? The preceding sentence is another question we intended to answer in this study. The reply to this question relates directly to a test of the second assumption of asperity models. For this purpose, we have computed the height histograms of the contacting regions $P(h)$, in which the height of every atom that is in contact is accounted for. The distributions linked to two different values of the roughness ratio and Hurst exponent are presented in Fig. 6. Given a fixed rms gradient value, the width of the distribution shows inverse proportionality with q_s/q_l. Furthermore, the center of the distribution shifts to higher values of h when q_s/q_l is decreased. This fact relates to the need to increase the fluctuations in the heights in order to maintain the same rms gradient once the fraction q_s/q_l has been reduced.

The main result revealed in Fig. 6 is the excellent description that a Gaussian function provides when fitting the $P(h)$'s. A Gaussian distribution for the heights in the contact regions corresponds flawlessly to the second assumption of asperity models. Yet we should remind the reader that the surface geometries considered in this work are always self-affine fractals. Thus, the heights of the contacting regions being Gaussian distributed should not come as a great surprise, if it is known *a priori* that the distribution of the heights for the full surface follows the same trend.

D. Hertzian contact versus total contact

The majority of engineering surfaces involve more than six decades in length scales. It is with the purpose of predicting their contact mechanics that asperity models have been developed. Lately [36], Persson has expressed concern about the applicability of the existing numerical methods to tackle the contact mechanics of such rough surfaces. While numerical techniques are still unable to address questions concerning surfaces with six orders of magnitude difference in roughness, approaches like our GFMD offer the possibility of studying with great accuracy the contact between surfaces with three decades in length scales. Thus, they represent suitable tools to shed light on the contact mechanics of systems of interest to engineers for microtechnological applications.

In the prior sections, we have focused our attention on unraveling the scaling laws obeyed by the normal forces on the contact clusters. We have also computed their area and height probability distributions, although no information has been provided to address how many of the atoms in contact belong to each scaling regime. Surely, an appealing issue relates to what percentage of the contact region is being occupied by the Hertzian clusters and what by the linear clusters.

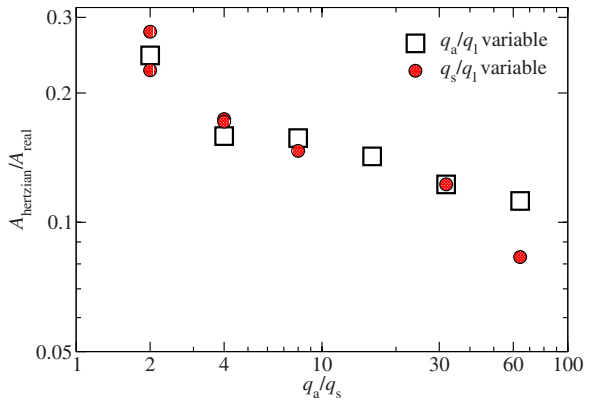

FIG. 7. (Color online) Relative percentage of contact: Contact area in the Hertzian regime versus total real area of contact, $A_{\mathrm{Hertzian}}/A_{\mathrm{real}}$. The open squares correspond to simulations in which the resolution fraction q_a/q_l was varied. Filled circles represent simulations with variable roughness ratio q_s/q_l. The data points on the right-hand side allowed us to obtain converged pressure distributions.

To characterize the contact morphology one needs to answer the question of how changes in the discretization ratio affect the nature of the contact. The path we have chosen to answer such a question is described as follows. Self-affine surfaces were created with roughness exponent and rms gradient identical to those of the ones employed to generate Fig. 2. Different random seeds were used. The effects of changing the discretization ratio are modeled using two alternative approaches. In the first one, changes in the discretization ratio q_a/q_s were achieved by varying the resolution fraction q_a/q_l such that q_s/q_l remained constant. This is equivalent to allowing the lattice constant a of the elastic sheet to change while keeping the surface profiles unaltered. In the second set of simulations, we varied q_s/q_l and kept q_a/q_l constant. For this second set of calculations the roughness at the smallest length scale q_s was variable while the lattice constant of the manifold stayed as $a=1$, as mentioned in Sec. II. It is important to emphasize that, even though both approaches accomplish the goal of making q_a/q_s variable, they are not equivalent.

The outcome of the calculations is shown in Fig. 7. The data points on the right-hand side of the plot $(q_a/q_s=64)$ correspond to simulations with values for the discretization ratio q_a/q_s suitable to attain converged pressure histograms $P(p)$. Converged pressure histograms ensure that the values of the relative area $A_{\mathrm{Hertzian}}/A_{\mathrm{real}}$ being reported do not change with further increase in the mesh resolution of the elastic sheet. Surprisingly, for a ratio of $q_a/q_s=64$, only a fraction of $\approx 10\%$ of the contact area can be found to belong to the Hertzian regime. Even if the roughness of the surface is increased up to three decades in length scales, $q_a/q_s=2$ (roughness ratio $q_s/q_l=2048$ and resolution ratio $q_a/q_l=4096$), the fraction in contact belonging to the Hertzian region raises only up to $\approx 30\%$. Due to the lack of convergence in the $P(p)$'s for these latter cases, the reported values of $A_{\mathrm{Hertzian}}/A_{\mathrm{real}}$ are expected to decrease when the resolution of the system is increased. Hence, we can conclude that, up to three decades in roughness, the clusters in the linear region dominate the real area of contact. Therefore, the assumption of asperity models when describing the contact as being formed by a large set of individual asperities satisfying the Hertzian contact mechanics is violated for surfaces with up to three decades in roughness.

Not having the possibility of achieving full convergence for systems with three decades of roughness prevented us from extrapolating our results to predict the value of the fraction $A_{\mathrm{Hertzian}}/A_{\mathrm{real}}$ for surfaces with six or more decades in length scales. Nevertheless, after analyzing the trend shown in Fig. 7, we anticipate a sustained increase in the number of clusters that belong to the Hertzian region as roughness of many more wavelengths is included within the description of the surface profiles. After all, several of the predictions of asperity models should resemble more the results of numerical simulations, if the self-affine surfaces under study have geometries that approach more closely those of regular engineering topographies.

IV. CONCLUSIONS

This paper has been developed with the aim of understanding the success of asperity models when describing the contact mechanics of randomly rough surfaces. To achieve such a goal, we have used Green's function molecular dynamics when studying the contact between self-affine surfaces. With the help of GFMD, we have tackled several questions concerning the validity of the assumptions and approximations made by asperity models.

We have shown how the contact region is formed by connected clusters with shapes that are determined by the competition between the discretization ratio q_a/q_s and the roughness ratio q_s/q_l. In the distribution of the normal forces L_c on the clusters, we have found the existence of two different scaling regimes according to the value of the cluster area A_c. Clusters with small areas satisfied a Hertzian-type law $L_c \sim A_c^{3/2}$, while larger clusters displayed a linear $L_c \sim A_c$ behavior. The coexistence of both regimes is independent of the relative area of contact A_{real}/A_0 and the roughness ratio q_s/q_l. Moreover, the critical area where the crossover between the regimes takes places proved to be a function of only the roughness at the short wavelength if the longitudinal dimension of the interface remained unchanged.

Addressing what percentage of the total area of contact corresponded to the Hertzian clusters and what percentage to the linear clusters composed another question we were interested in answering. The results of our simulations for self-affine surfaces with up to three decades in length scales demonstrated that the contact was dominated by the linear clusters ($A_{\mathrm{linear}}/A_{\mathrm{real}} \approx 70\%$ of the contact region), although the observed trend suggested a reduction in the above fraction when considering fractal surfaces with roughness similar to those of engineering systems. Therefore, the first assumption of asperity models might be well motivated for randomly rough surfaces with six or more orders of magnitude in the roughness.

We also computed the probability distribution of clusters sizes $P(A_c)$. In the Hertzian region, $P(A_c)$ remained nearly constant while within the linear regime it showed a power

law decay. Variations in the roughness exponent H of the surfaces barely changed the plateau in $P(A_c)$ for small cluster areas. Conversely, simulations corresponding to higher values of the Hurst exponent displayed changes in the tails of $P(A_c)$, such that the exponent of the power law shifted to smaller numbers in absolute units. Smaller values of H proved to limit the formation of larger clusters as expected from the scaling theory of fractal objects. Alternatively, changing the discretization ratio affected the behavior of $P(A_c)$ at small areas due to a lack of convergence in the pressure distributions $P(p)$. We find that including the elasticity on the flat surface and not on the rough geometry is the main cause for the existing differences between the power law exponent predicted by our model and the values observed in the calculations of Hyun *et al.* [23,24,26]

Lastly, with the aim of testing the second assumption of asperity models, we computed the height probability distribution $P(h)$ of the contacting zones. For the self-affine surfaces considered within this study, we found $P(h)$ to follow a Gaussian law. This fact corroborates the validity of asperity theories for elastic, nonadhesive contacts. Yet the prior result should not come as a surprise since we know that the surface heights are always Gaussian distributed in self-affine topographies.

ACKNOWLEDGMENTS

We would like to acknowledge NSERC for funding this work. We also thank Martin H. Müser and Mark O. Robbins for useful discussions.

[1] J. A. Greenwood and J. B. P. Williamson, Proc. R. Soc. London, Ser. A **295**, 300 (1966).
[2] C. Campañá, M. H. Müser, C. Denniston, Y. Qi, and T. A. Perry, J. Appl. Phys. **102**, 113511 (2007).
[3] B. N. J. Persson, O. Albohr, U. Tartaglino, A. I. Volokitin, and E. Tosatti, J. Phys.: Condens. Matter **17**, R1 (2005).
[4] R. Buzio, C. Boragno, F. Biscarini, F. B. De Mongeot, and U. Valbusa, Nature (London) **2**, 233 (2003).
[5] J. R. Barber, Proc. R. Soc. London, Ser. A **459**, 53 (2003).
[6] M. Ciavarella, V. Delfine, and G. Demelio, Wear **261**, 556 (2006).
[7] S. Cai and B. Bhushan, Wear **259**, 1408 (2005).
[8] K. L. Johnson, *Contact Mechanics* (Cambridge University Press, New York, 1985).
[9] H. Hertz, J. Reine Angew. Math. **92**, 156 (1882).
[10] M. Ciavarella, C. Murolo, and G. Demelio, Wear **261**, 1102 (2006).
[11] J. A. Greenwood and J. J. Wu, Meccanica **36**, 617 (2001).
[12] W. A. Bush, R. D. Gibson, and T. R. Thomas, Wear **35**, 87 (1975).
[13] J. F. Archard, Proc. R. Soc. London, Ser. A **243**, 190 (1957).
[14] R. A. Onions and J. F. Archard, J. Phys. D **6**, 289 (1973).
[15] D. J. Whitehouse and J. F. Archard, Proc. R. Soc. London, Ser. A **316**, 97 (1970).
[16] J. Krim and G. Palasantzas, Int. J. Mod. Phys. B **9**, 599 (1995).
[17] V. Bakolas, Wear **254**, 546 (2003).
[18] S. K. Chilamakuri and B. Bhushan, Proc. Inst. Mech. Eng. **212**, 19 (1998).
[19] N. Yu and A. A. Polycarpou, J. Tribol. **126**, 225 (2004).
[20] P. Meakin, *Fractals, Scaling and Growth far from Equilibrium* (Cambridge University Press, New York, 1997).
[21] L. Kogut and R. L. Jackson, J. Tribol. **128**, 213 (2006).
[22] C. Campañá, M. H. Müser, and M. O. Robbins, J. Phys.: Condens. Matter **20**, 354013 (2008).
[23] S. Hyun and M. O. Robbins, Tribol. Int. **40**, 1412 (2007).
[24] S. Hyun, L. Pei, J. F. Molinari, and M. O. Robbins, Phys. Rev. E **70**, 026117 (2004).
[25] G. G. Batrouni, A. Hansen, and J. Schmittbuhl, Europhys. Lett. **60**, 724 (2002).
[26] L. Pei, S. Hyun, J. F. Molinari, and M. O. Robbins, J. Mech. Phys. Solids **53**, 2385 (2005).
[27] M. Borri-Brunetto, B. Chiaia, and M. Ciavarella, Comput. Methods Appl. Mech. Eng. **190**, 6053 (2001).
[28] C. Campañá and M. H. Müser, Phys. Rev. B **74**, 075420 (2006).
[29] C. Campañá and M. H. Müser, Europhys. Lett. **77**, 38005 (2007).
[30] C. Yang, U. Tartaglino, and B. N. J. Persson, Eur. Phys. J. E **19**, 47 (2006).
[31] Y. Saito, J. Phys. Soc. Jpn. **73**, 1816 (2004).
[32] L. E. Landau and E. M. Lifshitz, *Theory of Elasticity* (Pergamon Press, London, 1970).
[33] C. Campañá, Phys. Rev. B **75**, 155419 (2007).
[34] J. Hoshen and R. Kopelman, Phys. Rev. B **14**, 3438 (1976).
[35] J. H. Dieterich and B. D. Kilgore, Tectonophysics **256**, 219 (1996).
[36] B. N. J. Persson, Surf. Sci. Rep. **61**, 201 (2006).
[37] B. N. J. Persson, J. Chem. Phys. **115**, 3840 (2001).